Molecular dynamics studies of nanoconfined water in clinoptilolite and heulandite zeolites

Nathan W. Ockwig,*[a] Randall T. Cygan,[a] Louise J. Criscenti[a] and Tina M. Nenoff[b]

Received 3rd August 2007, Accepted 15th November 2007
First published as an Advance Article on the web 10th December 2007
DOI: 10.1039/b711949f

The complete periodic series of alkali and alkaline earth cation variants (Li^+, Na^+, K^+, Rb^+, Cs^+, Mg^{2+}, Ca^{2+}, Sr^{2+}, and Ba^{2+}) of clinoptilolite (Si : Al = 5) and heulandite (Si : Al = 3.5) aluminosilicate zeolites are examined by large-scale molecular dynamics utilizing a flexible SPC water and aluminosilicate force field. Calculated hydration enthalpies, radial distribution functions, and ion coordination environments are used to describe the energetic and structural components of extra-framework species while power spectra are used to examine the intermolecular dynamics. These data are correlated to evaluate the impact of ion–zeolite, ion–water, and water–zeolite interactions on the behavior of nanoconfined water. Analysis of the correlated data clearly indicates that the charge density of extra-framework cations appears to have the greatest influence on librational motions, while the anionic charge of the framework (*i.e.* Si : Al ratios) has a lesser impact.

Introduction

Understanding the behavior of confined molecular species in microporous materials is a challenging topic which spans a wide variety of both experimental and theoretical arenas.[1–4] Nanoconfined water is arguably the most important species in porous materials to investigate because of its ubiquitous nature and tremendous impact across many industrially significant and interdisciplinary processes. The structural and dynamical properties of bulk water are now mostly well understood in a wide range of temperatures and pressures. It is also well known that the bulk properties of water are significantly modified when confined on a molecular scale.[5] However, despite its relatively simple molecular structure, the complex collective behavior of water remains a major challenge for current scientific understanding and levels of theory.[6] Quantifying the behavior of water in such confined systems is the first step towards understanding its role in macroscopic phenomena (*i.e.* species mobility and ion exchange) and ultimately provides the fundamental foundation for understanding, modifying and directing such properties. This is particularly true for zeolitic systems, where several focused studies on water in these systems have provided valuable insight to our greater understanding.[7–12]

Zeolites, derived from the Greek words *zein* "to boil" and *lithos* "a stone", are metastable microcrystalline aluminosilicate minerals which liberate occluded water molecules upon heating.[13] Largely defined by J. V. Smith[14a,b] and D. W. Breck,[14c] these framework-type minerals have structures that enclose channels and/or cavities which may be occupied by charge-compensating ions and water molecules. The enclosed species often possess significant freedom of movement which permits ion exchange and reversible dehydration behaviors. These aluminosilicate materials are built up from corner-sharing TO_4 tetrahedral units (where T is either Si or Al) with a generalized formula of $X_{x/n}[(AlO_2)_x(SiO_2)_y]$ where X is the charge-balancing counter-ion, n is the charge of the counter-ion, x is the number of charge-deficient alumina sites, and y is the number of charge-neutral silica sites. For every AlO_4 tetrahedron, the framework possesses a charge of -1 which must be balanced by the presence of additional extra-framework cations $X^{n+}_{x/n}$ that occupy the pores/channels of the zeolite. These cation species are quite often exchangeable as they are small enough to move through the zeolite network of channels and pores. The pores and channels result from progressive connections of two adjacent TO_4 units through a bridging oxygen atom to form T–O–T linkages. The wide angular flexibility of these T–O–T linkages ($\sim$100–180°) gives rise to topological and compositional zeolites variants. Zeolites are characterized by internal voids, channels, pores and/or cavities of well-defined size in the nanometer range, $\sim$4–13 Å, accessible through apertures of well-defined molecular dimensions.[15] Within these zeolitic pores, the behavior of water molecules is the direct response of complex equilibria among four distinct types of interactions: (1) H_2O–H_2O; (2) ion–H_2O; (3) H_2O–framework; and (4) ion–framework. The effect of these interactions (hydrogen bonds, electrostatics and ion–dipole) produce localized restrictions which alter the behavior of zeolite water from that of bulk water. An additional type of interaction, namely ion–ion electrostatic repulsions, may impact the water structure by spreading out the localized water attractors but this effect is probably less significant due to the effective screening of the zeolite

[a] *Geochemistry Department, Sandia National Laboratories, P.O. Box 5800, Albuquerque, NM 87185. E-mail: nockwig@sandia.gov; Tel: +1 (1)505 284 7681*
[b] *Surface and Interface Sciences Department, Sandia National Laboratories, P.O. Box 5800, Albuquerque, NM 87185, USA*

framework, and therefore was not investigated in this study. Spectroscopically, the molecular behavior of nanoconfined water is manifested by changes in the *intermolecular* librational/rotational (300–1100 cm^{-1}) modes and, to a lesser extent, the *intramolecular* bending ($\sim$1600 cm^{-1}) and stretching (3300–3700 cm^{-1}) modes. An overall analysis of the equilibrium dynamics of water in zeolites can be obtained through computational chemical analysis and correlation of power spectra obtained from the trajectories of large-scale molecular dynamics simulations.

In the last two decades, computer simulations, theoretical treatments and experiments on the structural and dynamic properties of water in different local microscopic environments have been performed on a wide variety of frequently used adsorbents such as clay minerals,[16] polymeric membranes,[17] various types of silica gels,[18] zeolites,[10] and activated charcoals.[19] The most prominent methods of extracting information on the structure and the intra- and inter-molecular behavior of bulk and confined water are molecular dynamics (MD),[20–25] neutron[26] and X-ray diffraction,[27] incoherent quasi-elastic and incoherent inelastic neutron scattering (IQENS and IINS respectively),[25,28–31] Raman scattering,[32] microwave and IR spectroscopies,[33] and nuclear magnetic resonance (NMR).[25,34] Many of these studies include multiple, and often complementary, methods to probe the role of water in connection with structural, dynamic and thermodynamic properties which have led to an impressive body of literature. However, there are numerous contradictory results which are continually challenging and improving our current levels of theory and understanding.

In this contribution, we investigate changes in the dynamic behavior of confined water molecules through their intermolecular interactions within the pores of the isostructural zeolitic frameworks—heulandite and clinoptilolite—and their counterbalancing cations. This highly variable system was specifically targeted to avoid the challenging topic of zeolite structural variations and their impact on H_2O interactions, but still address several fundamental basic science questions relating to the role of framework charge and cation type on confined water dynamics. Unlike the work of R. A. Jackson, C. R. A. Catlow and colleagues,[35] our studies focus on the rotational (and consequently spectroscopically-observable) behavior of water rather than hydration and dehydration processes, cation mobility or framework stability.

Model and simulation description

The models of these systems were constructed to encompass a large compositional phase space which facilitate the multi-dimensional analysis of the dynamic behavior of water in the heulandite class of zeolites over a range of compositional variants. Specifically, the trajectories generated from these MD simulations were analyzed to provide energetic properties (hydration enthalpies), structural characteristics (radial distribution functions and ion coordination environments), and dynamic behaviors (power spectra). Consistent with our recent simulation study of sodalite,[36] the framework atoms in our models do not have their positions fixed and the atomic interactions are evaluated through non-bonded potentials. The non-bonded van der Waals interactions are modeled with 6-12 Lennard-Jones potential terms[37] while the electrostatics are modeled through Coulombic potential terms and handled through an Ewald summation method.[38] This allows for a dynamically active zeolite framework which possesses some degree of flexibility without imposing the typical rigid body restrictions suffered by many prior zeolite models and allows for an increased computational efficiency without using explicitly defined framework-bonding parameters. This is further enhanced through the use of a flexible SPC-based (single point charge) water model,[39] which has harmonic bending and stretching terms included. These bending and stretching terms are the only explicitly-defined bonded interactions utilized in the force field. Lennard-Jones parameters (Table 1) for cation–water interactions were obtained from simulation studies of aqueous systems that utilized the SPC water model.[40] Geometric combination rules[41] were used to derive the off-diagonal Lennard-Jones interaction parameters for the various zeolite systems. The incorporation of combination rules and Lennard-Jones functions provides a relatively simple, yet accurate, method of evaluating the large number of atomic interactions associated with the simulations, and avoids the explicit requirements of Buckingham and other more complicated potential forms.

Heulandite and clinoptilolite are isostructural crystalline frameworks (both with the HEU framework type) with varying Si : Al ratios ranging from 2.5 to 6. Those with Si : Al ratios <4 are defined as heulandite (HEU), while those with ratios >4 are referred to as clinoptilolite (CLI). The structure itself is built up from rings of tetrahedral centers (T rings) which are interspersed by bridging oxygen atoms. In the HEU framework type, these rings define three distinct types of channels —one defined by 10T rings and two others by 8T rings—which are interconnected to form a layered array of channels (Fig. 1). One of the 8T channels (3.6 $\times$ 4.6 Å) and the 10T channel (3.1 $\times$ 7.5 Å) run parallel to the *c*-axis (Fig. 1C and 1A

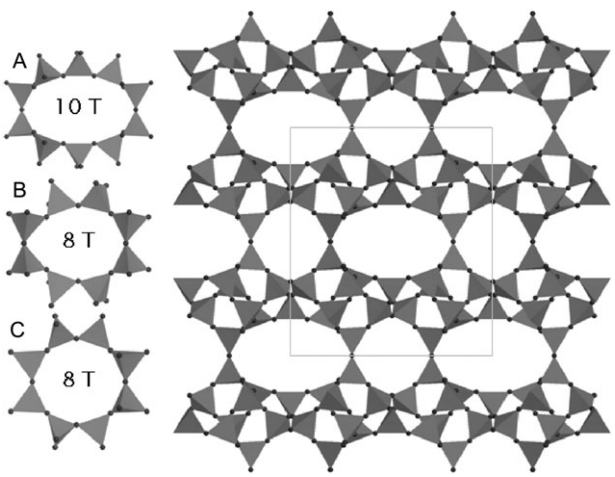

Fig. 1 The two-dimensional pore system created the intersection of a single 10T and two 8T channels. The 10T and 8T channels (A and C respectively) are parallel to the crystallographic *c*-axis and intersected by the remaining 8T channel (B) which is diagonal to the crystallographic *a*-axis. Polyhedra represent silicon (or aluminum) atoms while oxygen atoms are represented by small spheres.

Table 1 The partial charges, bond terms and 6-12 Lennard-Jones potentials of all species in the alkali and alkaline earth heulandite and clinoptilolite simulations

Species	Force field (FF) type	Charge/e	σ/nm	ε/kcal mol^{-1}
Water H	h*	+0.41	—	—
Water O	o*	−0.82	3.553	1.554×10^{-1}
Zeolitic Si	sz	+2.4	8.186	1.147×10^{-9}
Zeolitic Al	az	+1.4	0.831	$2.565 \times 10^{+3}$
Zeolitic O	oz	−1.2	12.654	2.305×10^{-8}
Ionic Li	li+	+1.0	4.726	9.026×10^{-7}
Ionic Na	na+	+1.0	2.553	1.115×10^{-1}
Ionic K	k+	+1.0	3.742	1.000×10^{-1}
Ionic Rb	rb+	+1.0	4.050	1.000×10^{-1}
Ionic Cs	cs+	+1.0	4.300	1.000×10^{-1}
Ionic Mg	mg++	+2.0	1.846	8.750×10^{-1}
Ionic Ca	ca++	+2.0	3.224	9.999×10^{-2}
Ionic Sr	sr++	+2.0	3.886	1.000×10^{-1}
Ionic Ba	ba++	+2.0	4.284	4.710×10^{-2}
Bond stretching parameters				
$E_{ij} = k_1(r - r_o)^2$				
Species i	Species j	k_1/kcal mol^{-1} Å^{-2}	r_o/Å	
o*	h*	553.9350	1.000	
Angle bending parameters				
$E_{ijk} = k_2(\theta - \theta_o)^2$				
Species i	Species j	Species k	k_2/kcal mol^{-1} rad^{-2}	θ_o/deg
h*	o*	h*	45.7530	109.47

respectively) while the remaining 8T channel (2.8 × 4.7 Å) is parallel to the a-axis (Fig. 1B) and intersects the first two channels to form an interconnected plane of channels. Both materials crystallize in the monoclinic space group $C2/m$ with slightly different unit cell parameters.[42]

For compatibility with the large-scale atomic/molecular massively parallel simulator (LAMMPS) molecular dynamics code,[43] the crystallographic symmetry restrictions were removed and the unit cell was transformed from monoclinic $C2/m$ to orthogonal $P1$ with unit cell parameters of $a = 15.92$, $b = 17.95$ and $c = 7.44$ Å. Our heulandite models have a fixed Si : Al substitution ratio of 3.5 whereas the clinoptilolite models have a Si : Al ratio of 5. This yields idealized heulandite and clinoptilolite formula (where X is a monopositive cation) of $X_8Si_{28}Al_8O_{72} \cdot 24H_2O$ and $X_6Si_{30}Al_6O_{72} \cdot 24H_2O$, respectively. The idealized structural formula includes the maximum pore/channel content of 24 water molecules. For better statistics, each model was expanded to include 20 unit cells [$2a \times 2b \times 5c$] to give a supercell of dimensions 31.83 × 35.90 × 37.18 Å containing a maximum of 2360 unique atoms when fully hydrated. The distribution of all aluminium sites throughout the supercell was randomly determined through virtual crystal approximation (the order–disorder subroutine of the Cerius^2 software)[44] following Löwenstein's substitution rule and held fixed across each model of the series.[45] Initial cation locations were extracted from crystallographic references,[46] while the initial water configurations were determined using a Cartesian hybrid Monte Carlo algorithm.[47]

All MD simulations were performed using the LAMMPS code[43] with the modified zeolite force field used previously (Table 1).[36] Simulations of the fully hydrated system using an isothermal–isobaric ensemble (NPT) revealed less than 0.2 Å (~1%) fluctuations along any given axis and on this basis we assume optimal unit cell parameters (Table 2). Equilibrations were performed with a canonical ensemble (NVT) over 250 ps at 300 K applying the Nosé–Hoover thermostat.[48] Radial distribution functions (RDF), running coordination numbers and energy evaluations were calculated from constant NVT production runs performed over 500 ps at 300 K, while power spectra were calculated through the Fourier transformation of velocity auto-correlation functions (VACF) that were compiled from 40 ps NVT trajectories with individual frames saved every 2 fs.[49]

Table 2 Comparison of experimental and calculated fully hydrated lattice parameters (Å). The Δ_{max} value represents the maximum deviation from the experimental cell parameters and their associated axis

	V/Å^3	a/Å	b/Å	c/Å	Δ_{max}/Å, axis
Exp.[a]	2107.87	15.81 (15)	17.92 (5)	7.40 (1)	—
Li–CLI	2106.52	15.83	17.91	7.43	+0.03, c
Na–CLI	2111.51	15.88	17.92	7.42	+0.07, a
K–CLI	2131.77	15.95	17.94	7.45	+0.14, a
Rb–CLI	2144.08	15.96	17.96	7.48	+0.15, a
Cs–CLI	2146.43	15.99	17.97	7.47	+0.18, a
Mg–CLI	2084.29	15.86	17.88	7.34	−0.06, c
Ca–CLI	2127.42	15.93	17.95	7.44	+0.12, a
Sr–CLI	2149.37	15.98	18.03	7.46	+0.17, a
Ba–CLI	2157.86	15.97	18.04	7.49	+0.16, a
Exp.[a]	2110.86	15.79 (58)	17.92 (21)	7.46 (13)	—
Li–HEU	2094.53	15.80	17.89	7.41	−0.05, c
Na–HEU	2105.66	15.87	17.93	7.40	+0.08, a
K–HEU	2121.85	15.94	17.94	7.42	+0.15, a
Rb–HEU	2143.41	15.98	17.98	7.46	+0.19, a
Cs–HEU	2140.39	15.97	17.99	7.45	+0.18, a
Mg–HEU	2111.35	15.87	17.93	7.42	+0.09, a
Ca–HEU	2131.80	15.92	17.95	7.46	+0.13, a
Sr–HEU	2149.34	15.96	17.98	7.49	+0.17, a
Ba–HEU	2152.36	15.97	17.97	7.50	+0.18, a

[a] Transformed from the experimental monoclinic $C2/c$ cell[42] to the orthogonal $P1$ simulation cell for LAMMPS compatibility.

Table 3 Experimental and calculated hydration enthalpies, ΔH_{hyd} (kcal mol^{-1})

	Li^+	Na^+	K^+	Rb^+	Cs^+	Mg^{2+}	Ca^{2+}	Sr^{2+}	Ba^{2+}
Ion (exp.)	−124	−97	−77	−71	−66	−459	−377	−345	−312
Ion (calc.)[a]	−127	−101	−69	−66	−62	−433	−358	−311	−314
CLI (calc.)[b]	−16.0	−14.2	−12.8	−12.4	−12.2	−98.8	−18.4	−17.6	−16.8
HEU (calc.)[b]	−18.1	−15.2	−13.0	−12.6	−11.9	−95.0	−15.5	−15.3	−15.1

[a] Calculated on a per mol ion basis with standard deviations of ±37 kcal mol^{-1}. [b] Calculated on a per mol H_2O basis with standard deviations of ±0.2 kcal mol^{-1}.

Molecular simulations in this study emphasize the dynamic behavior of the zeolites through the use of MD methods. Static calculations such as energy minimization were initially used in the development of the force field parameters and in the preliminary analysis of the zeolite framework structure. However, structural minimizations are limited to 0 K and fail to identify any dynamical aspects of cation hydration and of the zeolite framework which controls much of the molecular behavior at 300 K. We report dynamical averages for the lattice parameters for each of the zeolite systems and use MD to identify the key vibrational signatures associated with the dynamics of the pore water.

Results and discussion

We have performed large-scale molecular dynamics simulations on eighteen unique ion–zeolite pairs (Li–CLI, Na–CLI, K–CLI, Rb–CLI, Cs–CLI, Mg–CLI, Ca–CLI, Sr–CLI, Ba–CLI, Li–HEU, Na–HEU, K–HEU, Rb–HEU, Cs–HEU, Mg–HEU, Ca–HEU, Sr–HEU and Ba–HEU) using the procedure outlined above. To maintain charge neutrality, models containing divalent alkaline earth ions have only half the number of ions and these were placed in their respective crystallographically-defined positions.[46] For validation purposes we have compared experimental and calculated free-ion hydration enthalpies (Table 3), ion–O_{water} distances (Table 4) and coordination environments (Table 5) for all ions in this study.

Force field parameter validation

The force field was validated through comparison of experimental and calculated hydration enthalpies, ion–O_{water} distances and coordination environments, which are tabulated in the first two rows of Tables 3–5. Hydration enthalpies (ΔH_{hyd}) of the solvated free ions were calculated through the following equation:

$$\Delta H_{hyd}^{ion} = \langle U_{water+ion} \rangle - \langle U_{water} \rangle$$

where $\langle U_{water+ion} \rangle$ and $\langle U_{water} \rangle$ are the respective mean potential energies. Although most of the calculated ΔH_{hyd} values are slightly higher (Table 3) than those observed experimentally, Li^+ and Na^+ both show slightly decreased hydration enthalpies. The maximum deviations in these data occur for alkali K^+ and alkaline earth Sr^{2+}, which show elevated values of 8 (10.4%) and 34 (9.8%) kcal mol^{-1} respectively, relative to the experimental data. The distances between the water oxygen (O_{water}) and individual ions were extracted from RDF data and the coordination environments by integration of the resulting curves. The calculated ion–O_{water} distances from the bulk solvation simulations are generally in good agreement with experimental evidence with a majority of the distances being slightly overestimated but with Li^+ and Na^+ both being slightly underestimated, perhaps indicating a slight deficiency in the force field. Finally, the first coordination sphere of each ion shows good correlation with experimental values and very small deviations for the smaller, higher charge density ions and more significant deviations for the larger ions with lower charge densities. Despite the slight deviations in overall values, there is a strong agreement between experimental and calculated data. The periodic trends are still quite clear and show that the higher charge density divalent cations are much more strongly hydrated then their monovalent counterparts. The tabulated data in the first two rows of Tables 3–5 for hydration enthalpies, ion–O_{water} distances, and first coordination sphere environments illustrate these periodic trends quite clearly.

Table 4 Comparison of experimental and calculated ion–O_{water} distances (Å)

	Li^+	Na^+	K^+	Rb^+	Cs^+	Mg^{2+}	Ca^{2+}	Sr^{2+}	Ba^{2+}
Pure H_2O (exp.)[51]	2.10	2.41	2.80	2.92	3.14	2.07	2.33	2.60	2.90
Pure H_2O (calc.)	1.88	2.33	2.83	2.98	3.18	2.23	2.60	2.98	2.93
CLI–O_{water} (calc.)[a]	1.88	2.29	2.82	2.94	3.06	1.99	2.43	2.68	2.75
HEU–O_{water} (calc.)[a]	1.89	2.28	2.81	2.92	3.02	1.98	2.91	3.15	3.19

[a] Standard deviations are ±0.01 Å.

Radial distribution functions and hydration enthalpies

The overall hydration enthalpies in the zeolite–ion–water systems are composed of three types of energy contributions: the self solvation ($U_{water+water}$), individual ion hydration ($U_{ion+water}$), and zeolite hydration ($U_{framework+water}$) energies which cannot be decoupled without making significant assumptions. Therefore, we have elected to calculate these

Table 5 Experimental and calculated ion coordination environments (first sphere only) (total C. N. = total coordination number)

		Li^+	Na^+	K^+	Rb^+	Cs^+	Mg^{2+}	Ca^{2+}	Sr^{2+}	Ba^{2+}
	Ion–O_{water} (exp.)[51]	4.0	6.0	6.0	—	8.0	6.0	6.0	7.9	9.5
	Ion–O_{water} (calc.)	4.0	5.8	5.9	9.0	9.0	5.8	6.8	9.0	8.0
CLI	Ion–O_{water}	2.2	3.0	3.7	3.9	4.4	4.2	4.2	4.7	4.7
	Ion–$O_{framework}$	1.6	1.6	3.5	4.6	4.8	1.4	2.4	2.5	2.6
	Ion–O total C.N.	3.8	4.6	7.2	8.5	9.2	5.6	6.6	7.2	7.3
HEU	Ion–O_{water}	1.9	3.0	3.7	3.7	4.0	3.7	3.3	4.2	4.1
	Ion–$O_{framework}$	1.9	1.8	3.5	4.2	5.4	1.8	7.6	7.9	7.4
	Ion–O total C.N.	3.8	4.8	7.2	8.1	9.4	5.5	10.6	12.1	11.5

hydration enthalpies simply on a per mol H_2O basis through the following relation:

$$\Delta H_{\mathrm{hyd}}^{\mathrm{ion+framework}} = \frac{\langle U_{\mathrm{water+ion+framework}}\rangle - \langle U_{\mathrm{ion+framework}}\rangle}{n\mathrm{H_2O}}$$

where $\langle U_{\mathrm{water+ion+framework}}\rangle$ and $\langle U_{\mathrm{ion+framework}}\rangle$ are the respective mean potential energies while n is the total number of water molecules in the system. These values are compiled in the second two rows of Table 3. For comparison purposes, the data can be separated into four distinct types: CLI with alkali ions (CLI_{mono}), CLI with alkaline earth ions (CLI_{di}), HEU with alkali ions (HEU_{mono}) and HEU with alkaline earth ions (HEU_{di}). Each of these series shows that larger ions have less exothermic hydration enthalpies associated with the zeolite, and follow the trend $Li^+ > Na^+ > K^+ > Rb^+ > Cs^+$ for the alkalis and $Mg^{2+} \gg Ca^{2+} > Sr^{2+} > Ba^{2+}$ for the alkaline earths. In addition, the zeolite hydration enthalpies for the alkaline earth series are generally stronger than their counterparts in the alkali series. However, when we compare the hydration enthalpies for identical ions in the CLI *versus* HEU systems, we see some distinct differences. In the alkali series, the higher-charged HEU zeolite hydration enthalpies are more exothermic than those of the CLI system. This suggests that increasing the charge of the zeolite framework (by decreasing the Si : Al ratio) does indeed have an impact on the overall hydration enthalpy of the zeolite. However, when we examine the alkaline earth series we see that this trend is completely inverted with the lower-charged CLI zeolite having larger exothermic hydration enthalpies. When both observations are considered, the simulation data indicate that increasing ion charge density has a more significant impact on the overall hydration enthalpy than increasing the charge on the zeolite framework itself. This is consistent with the calculated ion–O_{water} distances where there are equivalent bond lengths across the entire alkali ion series regardless of the surrounding zeolite environment.

In the divalent HEU series we observe increased coordinating distances between the ion and the water oxygen (ion–O_{water}) whereas the CLI_{di} series shows decreased distances when compared with our bulk solvation results. Interestingly, the data for the CLI_{di} series universally deviate to shorter ion–water distances relative to the bulk solvation results while the entire HEU series shows increased bond distances with the exception of Mg^{2+}.

This can be rationalized by consideration of the overall charge on the zeolite framework. For example, in the CLI_{di} series the framework has a lower negative charge and therefore has less influence on the ion–O_{water} bond distances and therefore the ion–water interactions are dominant (*i.e.* short ion–water distances). Conversely, in the HEU system the framework has a greater negative charge and the ion–water interactions are subsequently disrupted by stronger ion–zeolite interactions at the charge-deficient Al sites which subsequently results in weaker ion–water interactions (*i.e.* greater ion–water distances).

Coordination environments

Analysis of the individual ion coordination environments focuses on the first coordination sphere. The coordination environments are detailed by accounting for contributions of $O_{framework}$ and O_{water} to the first coordination sphere of the ions in either CLI or the more negatively-charged HEU framework (Table 5). These contribution values are averaged over all ions within the 20 unit cell model and not each ion individually. As before, the data are separated into four groups (CLI_{mono}, CLI_{di}, HEU_{mono} and HEU_{di}) for comparison purposes. There is good consistency between the monovalent series and the calculated solvation values for the coordination numbers of Li^+, Rb^+ and Cs^+ in bulk water. In either zeolite, the coordination environment of Na^+ appears lowered while that of K^+ is elevated. Likewise, in the divalent series the coordination numbers for Mg^{2+} are close to the accepted value of six across all calculations, as are those for Ca^{2+} in CLI. In Sr– and Ba–CLI, the calculated ion coordination numbers are somewhat lower when compared with the reference solvation calculation. However, the HEU_{di} series shows significantly higher coordination numbers for Ca^{2+}, Sr^{2+} and Ba^{2+} than expected from the reference. Further analysis of the simulation data indicates that the $O_{framework}$ contribution to the first coordination sphere of any given ion is increased in the heulandite models. The increased $O_{framework}$ contribution appears to systematically lower the contribution of O_{water} to a small degree in the monovalent cases, and more extensively in the divalent cases. Simulation studies indicate that the level of contribution is largely determined by electrostatic considerations. Heulandite has a greater number of charge-deficient Al sites (a lower Si : Al ratio) than clinoptilolite, which increases the overall negative charge of the framework, specifically on the neighboring $O_{framework}$ sites. The effect is an increase in the interaction between the ion and zeolite. This evidence suggests a significant link between charge density (ion or framework) and the extent of ion hydration.

Power spectra and libration edge

The vibrational power spectrum of each hydrated ion–zeolite pair was calculated to study the intermolecular interactions of water, in particular the librational (rotational) region of the spectrum which occurs from 300 to 1100 cm^{-1}. On a molecular level, the broad peak(s) in this region of the spectrum have non-zero angular momentum components which are commonly referred to as the 'normal' wagging, twisting and bending modes of water. In cases where water is heavily restricted or isolated (through hydrogen bonding or sterics), these modes can become pronounced and are readily observed through IINS experiments.[50,53] However, despite significant efforts, their exact assignment (in terms of discrete wagging, twisting and bending) is still somewhat speculative because changes in the local environment can have dramatic effects on peak positions, widths and intensities. Generally though, frequency increases and peak width decreases as rotational restrictions are increased through hydrogen bonding or related steric effects. Additionally, the rotational modes are quite low in energy so thermal contributions result in extensive peak broadening which often requires IINS experiments to be performed at 10 K. In cases of heavily hydrated materials, the libration modes are not discrete due to the many different

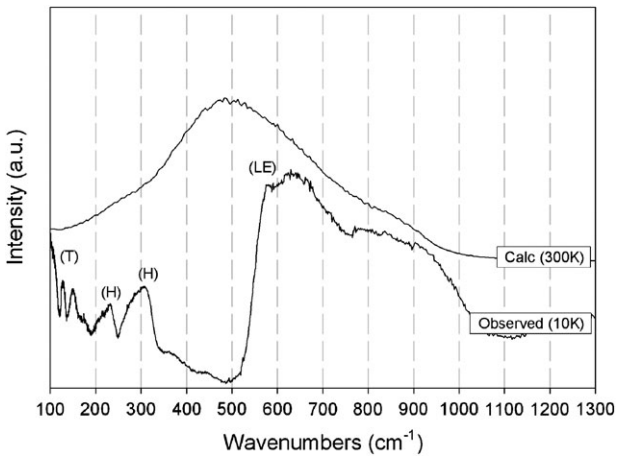

Fig. 2 The upper plot is the calculated power spectrum of liquid water at 300 K. The lower plot is the observed IINS spectrum for ice Ih at 10 K.[52] LE: librational edge, H: hydrogen-bond bending and stretching, T: translational modes.[53] (1 cm^{-1} = 0.1240 meV).

co-existing water configurations. This results in a confluence of discrete wagging, twisting and bending modes to form a single extremely broad ($\sim$500 cm^{-1}) feature which renders most data sets very difficult to interpret. Furthermore, because deconvolution of such broad features into individual components has questionable accuracy, the leading edge, often referred to as the librational edge, is commonly reported in the literature (Fig. 2).

The power spectra of confined water in each ion–zeolite system at 300 K were calculated and illustrated in Fig. 3. Water libration data of the monovalent (upper plots) *versus* divalent (lower plots) ion effects in the clinoptilolite series are compared against librational data from the heulandite series (monovalents and divalents). Comparison across the monovalent series (Fig. 3A and C) shows strikingly similar power spectra (on a per ion basis) and nearly identical trends in libration shifts which increase frequency as a function of decreasing ion charge density ($Li^+ < Na^+ < K^+ < Rb^+ < Cs^+$). Comparison across the divalent series (Fig. 3B and D) reveals a completely different trend for the CLI series *versus* the HEU series. In the CLI_{di} series, a shift to lower frequency as a function of increasing ion charge density ($Ba^{2+} < Sr^{2+} < Ca^{2+} < Mg^{2+}$) is observed. However in the HEU_{di} series, a slightly increase in librational frequencies as ion charge density decreases ($Mg^{2+} < Ca^{2+} < Sr^{2+} < Ba^{2+}$) is observed. Within the CLI series (Fig. 3A and B) opposite trends in the libration shifts are observed. CLI_{mono} shows an increasing trend while CLI_{di} shows a decreasing trend in frequency shifts as a function of the ion charge densities. Within the HEU series (Fig. 3C and D) a similar trend of librational shifts to higher frequencies as a function of decreasing ion charge

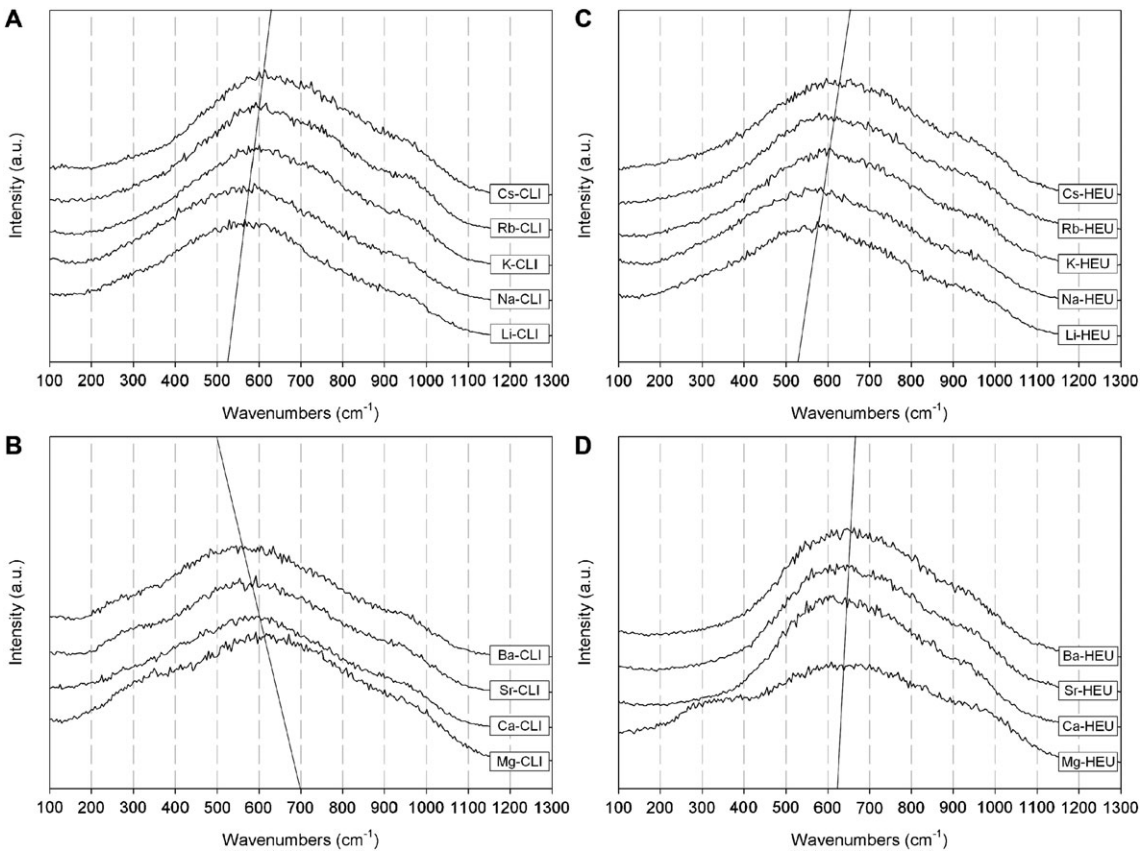

Fig. 3 Librational region of the power spectra for water at 300 K confined in: (A) clinoptilolite with alkali ions, (B) clinoptilolite with alkaline earth ions, (C) heulandite with alkali ions, and (D) heulandite with alkaline earth ions. Lines indicate the general trend in the shift in peak positions.

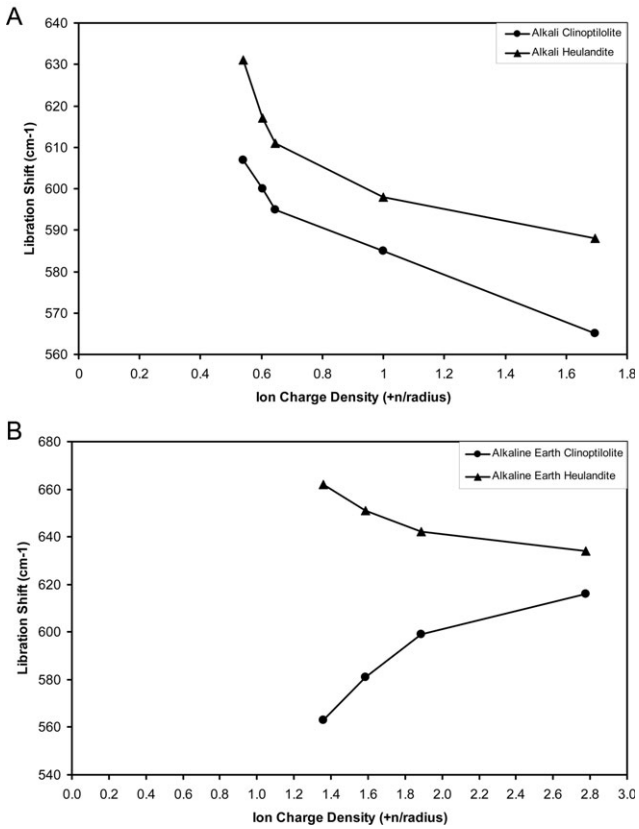

Fig. 4 Librational shifts (cm^{-1}) of (A) the alkali and (B) alkaline earth series *versus* ion charge density. Clinoptilolite data represented by filled circles and heulandite data represented by filled triangles.

density is observed, albeit with a smaller magnitude in the HEU_{di} series.

Further examination of the libration shifts (Fig. 4) clearly indicates that the rotations of nanoconfined water in a charged zeolite are affected by both the cationic charge density and the anionic field strength of the zeolite itself. In Fig. 4A, the shifts are higher in magnitude for the more negatively-charged heulandite which indicates that the greater electrostatic field of the zeolite is producing more restricted rotations. This effect becomes more pronounced with decreasing cationic charge density. In Fig. 4B, the alkaline earth series exhibits the same trend for the heulandite system. However, the trend starts at higher initial wavenumber indicating that the higher cationic field strength is further restricting the rotational motion of confined water. Finally, the alkaline earth clinoptilolite series (Fig. 4B) exhibits a unique trend when compared with the others. Here the rotational motion of the confined water increases (as indicated by decreasing wavenumbers) with decreasing charge density. The explanation of this trend remains speculative. However, the data suggest that it arises from a shift in ion–water–zeolite equilibria towards the stronger ion–water interactions over the diminished ion–zeolite or zeolite–water interactions. Another mitigating factor to consider in this explanation is the contribution of water–water and water–zeolite interactions in pores where there are no or very few ions present (*i.e.* alkaline earth clinoptilolite).

The cumulative interpretation of the power spectra suggests several key elements affecting the dynamic behavior of nanoconfined water. First, both the cation charge density and the anionic field strength (*i.e.* the Si : Al ratio) have a significant impact on the dynamics. Second, the balance between cation charge density and framework field strength has a marked impact on the librational signatures of a given zeolite system. The data clearly show that alteration of the ion–water–zeolite equilibria conditions changes the dynamic intermolecular behavior of nanoconfined water and results in different solvating environments for cations within a negatively-charged zeolitic pore.

Conclusions

We have examined the complete alkali and alkaline earth series of cation variants of clinoptilolite (Si : Al = 5) and heulandite (Si : Al = 3.5) using large-scale molecular dynamics (MD) utilizing a flexible SPC water and aluminosilicate force field. Hydration enthalpies, radial distribution functions and local ion coordination environments demonstrate the energetic and structural influence of zeolite electrostatic fields (Si : Al ratios). These contributions to the dynamic intermolecular behavior of nanoconfined water are manifested in the librational region of the power spectra. Correlation of these data confirms the importance of ion–zeolite, ion–water and water–zeolite equilibria on the rotational behavior of water. Analysis of these data clearly indicates that the charge density of extra-framework cations has the greater influence on librational motions, while the anionic charge of the framework (*i.e.* Si : Al ratios) has a lesser impact. The combined influence of these two variables provides a basic foundation to understand the influence of cation charge density and anionic field strength, and the delicate balance between these electrostatic fields. Furthermore, the modifications of the ion–water–zeolite equilibria conditions changes the intermolecular behavior of nanoconfined water, which is manifested through shifts in the libration (rotational) region of the power spectra. Future investigation necessarily includes (1) comparison of our simulated power spectra with the observed experimental IINS data,[52] (2) thermodynamic studies of ion-exchange and hydration processes, and (3) structural analysis of hydrogen-bonded water networks in the zeolite systems as a function of cation identity and degree of Si/Al substitution.

Acknowledgements

We would like to thank Jeffery A. Greathouse and James P. Larentzos for numerous insightful discussions and three anonymous reviewers for their helpful suggestions. This work was fully supported by the Laboratory Directed Research and Development (LDRD) program of Sandia National Laboratories. Sandia National Laboratories is a multiprogram laboratory operated by Sandia Corporation, a Lockheed Martin Company, for the United States Department of Energy's National Nuclear Security Administration under contract DE-AC04-94AL85000.

References

1 J. Klafter, A. Blumen and J. M. Drake, in *Relaxation and Diffusion in Restricted Geometry*, ed. J. Klafter and J. M. Drake, Wiley, New York, 1989.
2 J. A. Rupley and G. Careri, *Adv. Protein Chem.*, 1991, **41**, 37.
3 M. Arndt, R. Stannarius, W. Gorbatschow and F. Kremer, *Phys. Rev. E*, 1996, **54**, 5377.
4 *Proceedings of the First International Workshop of Dynamics in Confinement*, ed. B. Frick, R. Zorn and H. Buttner, EDP Science, Les Ulis, France, 2000.
5 (*a*) Special Section on Water in Confined Geometries, ed. M. Rovere, *J. Phys.: Condens. Matter*, 2004, **16**, S5297; (*b*) V. Crupi, D. Majolino and V. Venuti, *J. Phys.: Condens. Matter*, 2004, **16**, S5297; (*c*) J. Swenson, *J. Phys.: Condens. Matter*, 2004, **16**, S5317; (*d*) J. Puibasset and R. J. M. Pellenq, *J. Phys.: Condens. Matter*, 2004, **16**, S5329; (*e*) I. Brovchenko, A. Geiger and A. Oleinikova, *J. Phys.: Condens. Matter*, 2004, **16**, S5345; (*f*) R. Zangi, *J. Phys.: Condens. Matter*, 2004, **16**, S5371; (*g*) P. Jedlovsky, *J. Phys.: Condens. Matter*, 2004, **16**, S5389; (*h*) L. Liu, A. Faraone, C. Y. Mou, C. W. Yen and S. H. Chen, *J. Phys.: Condens. Matter*, 2004, **16**, S5403; (*i*) J. Klein, U. Raviv, S. Perkin, N. Kampf, L. Chai and S. Giasson, *J. Phys.: Condens. Matter*, 2004, **16**, S5437; (*j*) B. Webber and J. Dore, *J. Phys.: Condens. Matter*, 2004, **16**, S5449.
6 C. A. Angell, in *Water: A Comprehensive Treatise*, ed. F. Franks, Plenum Press, New York, 1981.
7 T. Mizota, N. Satake, K. Fujiwara and N. Nakayama, in *Steam, Water, and Hydrothermal Systems: Physics and Chemistry Meeting the Needs of Industry*, *Proceedings of the 13th ICPWS*, ed. P. R. Tremaine, P. G. Hill, D. E. Irish and P. V. Balakrishnan, NCR Research Press, Ottawa, Ontario, 2000.
8 I. A. Beta, H. Bohling and B. Hunger, *Phys. Chem. Chem. Phys.*, 2004, **6**, 1975.
9 H. Jobic, A. Tuel, M. Krossner and J. Sauer, *J. Phys. Chem.*, 1996, **100**, 19545.
10 V. Crupi, D. Majolino, P. Migliardo, V. Venuti, U. Wanderlingh, T. Mizota and M. Telling, *J. Phys. Chem. B*, 2004, **108**, 4314.
11 C. M. B. Line and G. J. Kearley, *J. Chem. Phys.*, 2000, **112**, 9058.
12 C. M. B. Line and G. J. Kearley, *Chem. Phys.*, 1998, **234**, 207.
13 A. F. Cronstedt, *Kongl Vetenskaps Academiens Handlingar Stockholm*, 1756, **17**, 120.
14 (*a*) J. V. Smith, *Mineral. Soc. Am., Spec. Pap.*, 1963, **1**, 281; (*b*) J. V. Smith, in *Zeolite Chemistry and Catalysis*, ed. J. A. Rabo, American Chemical Society, Washington DC, 1976; (*c*) D. W. Breck, *Zeolite Molecular Sieves*, Wiley, New York, 1974.
15 F. M. Higgins, N. H. de Leeuw and S. C. Parker, *J. Mater. Chem.*, 2002, **12**, 124.
16 A. K. Soper, in *Hydrogen Bond Network, NATO ASI Series C: Mathematical and Physical Science*, ed. M. C. Bellissent-Funel and J. C. Dore, Kluwer Academic, Dordecht, 1994.
17 P. M. Wiggins, *Prog. Polym. Sci.*, 1988, **13**, 1.
18 V. Crupi, D. Majolino, P. Migliardo, V. Venuti, U. Wanderlingh, T. Mizota and M. Telling, *J. Phys. Chem. B*, 2002, **106**, 10884.
19 M. C. Bellissent-Funel, R. Dorbez-Sridi and L. Bosio, *J. Chem. Phys.*, 1996, **104**, 1.
20 P. Gallo, M. A. Ricci and M. Rovere, *J. Chem. Phys.*, 2002, **116**, 342.
21 P. Gallo, M. Rapinesi and M. Rovere, *J. Chem. Phys.*, 2002, **117**, 369.
22 S. Murad, W. Jia and M. Krishnamurthy, *Mol. Phys.*, 2004, **102**, 2103.
23 P. Demontis, G. Stara and G. B. Suffritti, *J. Chem. Phys.*, 2004, **120**, 9233.
24 K. Shirono, A. Endo and H. Daiguji, *J. Phys. Chem. B*, 2005, **109**, 3446.
25 T. M. Nenoff, N. W. Ockwig, R. T. Cygan, T. M. Alam, K. Leung, J. D. Pless, H. Xu, M. A. Hartl and L. L. Daemen, *J. Phys. Chem. C*, 2007, **111**, 13212.
26 V. Crupi, D. Majolino, P. Migliardo, V. Venuti and M. C. Bellissent-Funel, *Mol. Phys.*, 2003, **101**, 3323.
27 A. Fourzi, R. Dorbez-Sridi and M. Oumezzine, *J. Chem. Phys.*, 2002, **116**, 791.
28 A. I. Kolesnikov and J. C. Li, *Phys. B*, 1997, **234**, 34 and references therein.
29 M. C. Bellissent-Funel, J. Lal and L. Bosio, *J. Chem. Phys.*, 1993, **98**, 4246.
30 V. Crupi, D. Majolino, P. Migliardo, V. Venuti and A. J. Diaonoux, *Appl. Phys. A*, 2002, **74**, S555.
31 F. Venturini, P. Gallo, M. A. Ricci, A. R. Bizzari and S. Cannistraro, *J. Chem. Phys.*, 2001, **114**, 10010.
32 V. Crupi, S. Magazu, G. Maisano, D. Majolino and P. Migliardo, *J. Mol. Liq.*, 1999, **80**, 133.
33 U. Kaatze and V. Uhlendorf, *Z. Phys. Chem., Neue Folge*, 1981, **126**, 151.
34 C. F. Polnazek and R. G. Bryant, *J. Chem. Phys.*, 1984, **81**, 4038.
35 (*a*) R. A. Jackson and C. R. A. Catlow, *Mol. Simul.*, 1988, **1**, 207; (*b*) G. Ooms, R. A. van Santen, C. J. J. den Ouden, R. A. Jackson and C. R. A. Catlow, *J. Phys. Chem.*, 1988, **92**, 4462; (*c*) G. Aloisi, P. Barnes, C. R. A. Catlow, R. A. Jackson and A. J. Richards, *J. Chem. Phys.*, 1990, **93**, 3573; (*d*) Y. M. Channon, C. R. A. Catlow, A. M. Gorman and R. A. Jackson, *J. Phys. Chem. B*, 1998, **102**, 4045; (*e*) M. Johnson, D. O'Connor, P. Barnes, C. R. A. Catlow, S. L. Owens, G. Sankar, R. Bell, S. J. Teat and R. Stephenson, *J. Phys. Chem. B*, 2003, **107**, 942.
36 (*a*) E. C. Moloy, R. T. Cygan, F. Bonhomme, D. M. Teter and A. Navrotsky, *Chem. Mater.*, 2004, **16**, 2121; (*b*) O. Teleman, B. Jonsson and S. Engstrom, *Mol. Phys.*, 1987, **60**, 193.
37 J. E. Lennard-Jones, *Proc. Phys. Soc., London*, 1931, **43**, 461.
38 L. M. Fraser, W. M. C. Foulkes, G. Rajagopal, R. J. Needs, S. Kenny and A. J. Williamson, *Phys. Rev. B*, 1996, **53**, 1814.
39 (*a*) H. J. C. Berendsen, J. P. M. Postma, W. F. van Gunsteren and J. Hermans, in *Intermolecular Forces*, ed. B. Pullmann, Reidel, Dordrecht, 1981, p. 331; (*b*) G. W. Robinson, S.-B. Zhu, S. Singh and M. W. Evans, in *Water in Biology, Chemistry and Physics: Experimental Overviews and Computational Methodologies*, World Scientific, Singapore, 1996.
40 (*a*) D. E. Smith and L. X. Dang, *J. Chem. Phys.*, 1994, **100**, 3757; (*b*) J. Aqvist, *J. Phys. Chem.*, 1990, **94**, 8021; (*c*) S. Koneshan, J. C. Rasaiah, R. M. Lynden-Bell and S. H. Lee, *J. Phys. Chem. B*, 1998, **102**, 4193; (*d*) B. J. Palmer, D. M. Pfund and J. L. Fulton, *J. Phys. Chem.*, 1996, **100**, 13393.
41 T. A. Halgren, *J. Am. Chem. Soc.*, 1992, **114**, 7827.
42 Clinoptilolite: a = 17.66 (7), b = 17.92 (5), c = 7.40 (1) Å, and β = 116.43 (14)°. Heulandite: a = 17.62 (24), b = 17.92 (21), c = 7.46 (13) Å, and β = 116.34 (53)°.
43 (*a*) S. J. Plimpton, *J. Comput. Phys.*, 1995, **117**, 1; (*b*) S. J. Plimpton, R. Pollock and M. Stevens, in *Proceedings of the Eighth SIAM Conference on Parallel Processing for Scientific Computing*, ed. M. Heath, V. Torczon, G. Astfalk, P. E. Bjørstad, A. H. Karp, C. H. Koebel, V. Kumar, R. F. Lucas, L. T. Watson and D. E. Womble, SIAM, Minneapolis, MN, USA, 1997; (*c*) The LAMMPS code is freely available from http://lammps.sandia.gov.
44 B. Winkler, C. J. Pickard and V. Milman, *Chem. Phys. Lett.*, 2002, **362**, 266.
45 W. Löwenstein, *Am. Mineral.*, 1954, **39**, 92.
46 P. Yang and T. Armbruster, *J. Solid State Chem.*, 1996, **123**, 140.
47 (*a*) Implemented through the 'Amorphous Cell' module of Materials Studio, Accelrys, http://www.accelrys.com/products/mstudio; (*b*) B. M. Forrest and U. W. Suter, *J. Chem. Phys.*, 1994, **101**, 2616 and references therein.
48 (*a*) S. Nosé, *Mol. Phys.*, 1984, **52**, 255; (*b*) W. G. Hoover, *Phys. Rev. A*, 1985, **31**, 1695; (*c*) M. P. Allen and A. Tildesley, *Computer Simulation of Liquids*, Oxford University Press, New York, 1987.
49 (*a*) Y. Li, S.-T. Lin and W. A. Goddard, III, *J. Am. Chem. Soc.*, 2004, **126**, 1872; (*b*) G. Maurin, R. G. Bell, S. Devautour, F. Henn and J. C. Giuntini, *Phys. Chem. Chem. Phys.*, 2004, **6**, 182; (*c*) M. Praprotnik, D. Janezic and J. Mavri, *J. Chem. Phys. A*, 2004, **108**, 11056.
50 J. C. Li, *J. Chem. Phys.*, 1996, **105**, 6733.
51 H. Ohtaki and T. Radnai, *Chem. Rev.*, 1993, **93**, 1157.
52 Data collected at LANL-LANSCE on the Filter Difference Spectrometer (FDS) beamline.
53 J. C. Li and D. K. Ross, *Nature*, 1993, **365**, 327.